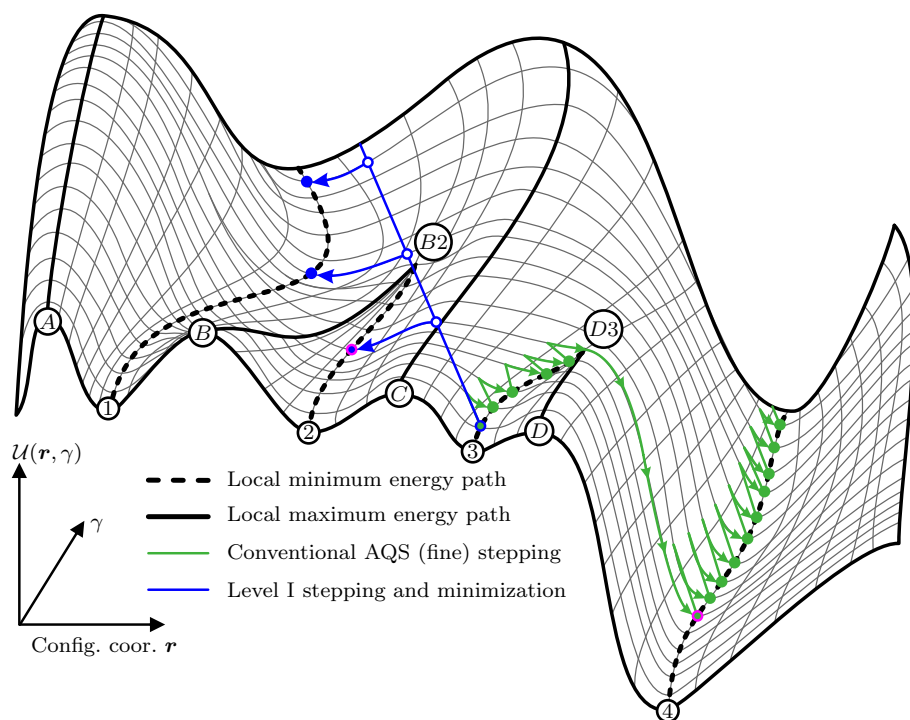


Graphical Abstract

Parallel athermal quasistatic deformation stepping of molecular systems

Maximilian Reihn, Franz Bamer, Benjamin Stamm



Highlights

Parallel athermal quasistatic deformation stepping of molecular systems

Maximilian Reihn, Franz Bamer, Benjamin Stamm

- We propose a novel two-level athermal parallel stepping scheme that accelerates quasistatic molecular simulations.
- With the help of multi-threading and characteristics of the potential energy surface of molecular systems, we perform athermal deformation protocols at different deformation states simultaneously.
- We achieve consistent computational speed-ups, with an average acceleration factor of between 3.0 and 6.62 depending on the number of processors used, compared to conventional athermal quasistatic deformation methods, while preserving the same level of accuracy.

Parallel athermal quasistatic deformation stepping of molecular systems

Maximilian Reihn^a, Franz Bamer^b, Benjamin Stamm^a

^a*Institute for Applied Analysis and Numerical Simulation, University Stuttgart, Pfaffenwaldring
57, Stuttgart, 70569, Baden-Württemberg, Germany*

^b*Institut für Allgemeine Mechanik, Eilfschornsteinstraße 16, Aachen, 52062, Nordrhein-Westfalen, Germany*

Abstract

The athermal quasistatic deformation method provides an elegant solution to overcome the limitation of short time spans in molecular simulations. It provides overdamped conditions, allowing for the extraction of purely structural responses in the absence of thermal vibration. However, it requires computationally expensive sequences of affine deformation followed by minimization of the potential energy to incrementally find the path in the potential energy landscape that corresponds to the correct solution trajectory. Therefore, we propose an athermal parallel stepping scheme that significantly improves the computational time necessary to find the correct solution trajectory using a multi-thread approach. Our approach proposes athermal stepping at two levels. Level I stepping provides a sequence of initial guesses at large increments by affine deformation of the system and land-marking anchor points on the potential energy landscape. Level II stepping performs a set of individual finely resolved athermal quasistatic deformation steps between the inherent structures of the initial level I guesses executed in parallel. The evaluated candidate trajectory is then verified by consecutively comparing the configuration of every last level II result with the corresponding inherent structure of the level I guesses at the same strain states. If the two configurations are not equivalent, the solution must be rejected and recalculated from this point. Rigorous numerical testing with 4, 8, 16 and 32 parallel threads demonstrates that our method achieves computational speed-ups of factors ranging from 1.49 to 27.09, with averages of 3.0 to 6.62 depending on the number of threads, while maintaining simulation accuracy, offering a powerful new tool for athermal molecular simulations.

Keywords: Parallel computing, Molecular dynamics, Athermal quasistatic deformation, Potential energy landscape, Disordered systems, Glasses

1. Introduction

Molecular models provide valuable insights into the structure-property relationship of nanostructures and give us a general idea of how materials respond to external deformation [1]. In particular, mechanical phenomena, such as fracture, originate from the nanoscale and span multiple orders of magnitude, connecting nanoscale inelastic behavior to larger-scale dynamics [2].

Molecular models are built on the assumption that atoms are modeled as point masses, while appropriate potential functions describe their interactions. They allow for significantly larger models compared to quantum mechanical frameworks and often serve as a bridge to continuum mechanical descriptions [3]. However, physically meaningful studies require a large number of atoms, so the dimension of the problem is high, and the number of interactions between the particles to be considered is even higher. These issues limit the application of molecular models and make an overall efficient implementation challenging [4, 5].

Significant effort has been devoted to overcoming this issue, with proposals that can be categorized into two groups. The first group includes methods that optimize the distance evaluations and interaction evaluation by introducing cutoff radii, Verlet lists, and Linked Cell lists [1, 6]. The second group of methods focuses on multi-threading, i.e., distributing the computation effort within several tasks that are executed individually [7, 8]. Such parallelization can be performed through atom-wise decomposition, force decomposition, and spatial decomposition, whereas the third strategy has shown the highest efficiency for molecular problems [9, 10].

Notably, such strategies accelerate computation during a single incremental calculation step, typically performed during a time integration algorithm or a procedure that minimizes the potential energy. Due to the high dimensionality of molecular models, explicit time integration schemes, such as the Velocity Verlet algorithm [11, 12], have been established as the preferred algorithms since they neither require iterations during every step nor the assembly and subsequent inversion of the Hessian matrix. An essential disadvantage of these methods is, however, that the computation time step chosen must not be larger than the highest eigenfrequency of the linearized system at the current deformation state [13, 14]. Effectively, this value is proportional to the vibration period of the strongest atomic bonds, forcing one to choose calculation time steps in the range of femtoseconds. Consequently, a disproportionately high number of calculation steps are necessary to cover a certain simulation time period, which strongly limits the possible simulation time span. Therefore, molecular simulations are not only limited in terms of the system size but also in terms of the simulation time window, greatly hindering decisions for possible up-scaling.

When performing mechanical deformation, the athermal quasistatic simulation or zero-temperature method [15] alleviates the limiting time problem to some extent, as it allows for infinitely slow mechanical deformation in the absence of Brownian motion. It describes an overdamped system, continuously following the minimum configuration of the atomic system. However, it requires subsequent minimization procedures during every deformation step, leading again to a limitation due to computational effort. Thus, this paper proposes an in-parallel athermal quasistatic stepping algorithm using multi-processor machines. Notably, our method provides exact simulation results, saving computational time compared to conventional athermal quasistatic deformation stepping while being flexible enough s.t. the force-evaluation can be further parallelized on top.

The paper is organized as follows. Firstly, the athermal quasistatic deformation method is introduced, including the benchmark example used to demonstrate the in-parallel deformation stepping method. Subsequently, we present a new parallel computing approach, accompanied by rigorous studies that demonstrate the computational benefits compared to the conventional athermal quasistatic deformation method. Finally, conclusions are drawn and an outlook for future work is provided.

2. Athermal quasistatic deformation

Being exclusively interested in the structural response of the material, we investigate mechanical deformation without considering any thermal vibrations [16, 17, 3], so the configuration remains in a local minimum of the potential energy landscape. Effectively, we are investigating materials at zero temperature. Such an assumption remains meaningful as long as we consider materials at temperatures significantly lower than the melting temperature or, in the particular case of glasses, considerably lower than the glass transition temperature [18]. We confine a total number of N atomic particles into a d -dimensional simulation cell whose geometry is defined by the second order Bravais tensor on a reference cell $\hat{\mathbf{H}} = [\hat{\mathbf{h}}_1, \hat{\mathbf{h}}_2]$ for $d = 2$ and $\hat{\mathbf{H}} = [\hat{\mathbf{h}}_1, \hat{\mathbf{h}}_2, \hat{\mathbf{h}}_3]$ for $d = 3$, where $\hat{\mathbf{h}}_1, \hat{\mathbf{h}}_2$ and $\hat{\mathbf{h}}_3$ refer to the linearly independent Bravais vectors [19]. Periodic boundary conditions are applied in the direction of all three Bravais vectors, although the method proposed in this paper also applies to systems without periodic boundary conditions [20].

External deformation is performed by altering the shape of the simulation cell through the manipulation of Bravais vectors, assembly of the Bravais tensor, and adjustment of atomic positions. We define the current configuration $\mathbf{H}^{(\gamma)}$, which was deformed by an affine deformation parameter $\gamma \in \mathbb{R}$ from the reference configuration $\hat{\mathbf{H}}$. The deformation is done incrementally by multiplying the deformation tensor $\mathbf{F}^{(\Delta\gamma)}$ such that $\mathbf{H}^{(\gamma+\Delta\gamma)} = \mathbf{F}^{(\Delta\gamma)} \mathbf{H}^{(\gamma)}$. For $\gamma = 0$ the current configuration is the reference configuration, meaning $\mathbf{H}^{(\gamma)} = \hat{\mathbf{H}}$. Mechanical deformation is induced by altering the Bravais tensors, written as:

$$\mathbf{F}^{(\Delta\gamma)} = \mathbf{H}^{(\gamma+\Delta\gamma)} \left(\mathbf{H}^{(\gamma)} \right)^{-1}. \quad (1)$$

Atoms are defined by their position vectors within the configuration

$$\mathbf{r}_i \in \text{conv}(\mathbf{H}) := \text{conv} \left(\left\{ \sum_{j=1}^d \alpha_j \mathbf{h}_j \mid \forall (\alpha_1, \dots, \alpha_d) \in \{0, 1\}^d \right\} \right) = \text{conv}(\{\mathbf{H}\boldsymbol{\alpha} \mid \forall \boldsymbol{\alpha} \in \{0, 1\}^d\})$$

for all $i = 1, \dots, N$ where we stack all the atomic positions to one concatenated position vector $\mathbf{r} \in \text{conv}(\mathbf{H})^N := \text{conv}(\mathbf{H}) \times \dots \times \text{conv}(\mathbf{H}) \subset \mathbb{R}^{dN}$. The expression $\text{conv}(\mathbf{H})$ describes a unit square when $\mathbf{H} = [(0, 1), (1, 0)]$.

The mapping \mathbf{F} is applied to a single particle i 's position as follows:

$$\begin{aligned} \mathbf{F}^{(\Delta\gamma)} : \text{conv}(\mathbf{H}^{(\gamma)}) &\rightarrow \text{conv}(\mathbf{H}^{(\gamma+\Delta\gamma)}), \\ \mathbf{r}_i &\mapsto \mathbf{F}^{(\Delta\gamma)} \mathbf{r}_i. \end{aligned} \quad (2)$$

The deformation mapping for the entire N -particle system is written as:

$$\begin{aligned} \left(\mathbf{F}^{(\Delta\gamma)} \right)^N : \text{conv}(\mathbf{H}^{(\gamma)})^N &\rightarrow \text{conv}(\mathbf{H}^{(\gamma+\Delta\gamma)})^N, \\ \mathbf{r} &\mapsto \begin{bmatrix} \mathbf{F}^{(\Delta\gamma)} & & \mathbf{0} \\ & \ddots & \\ \mathbf{0} & & \mathbf{F}^{(\Delta\gamma)} \end{bmatrix} \mathbf{r}. \end{aligned} \quad (3)$$

It will be apparent from context if $\mathbf{F}^{(\Delta\gamma)}$ or $(\mathbf{F}^{(\Delta\gamma)})^N$ is applicable hence, we drop the superscript N . In the following, we observe the system from the Lagrangian perspective [21], which means that we formulate our equations with variables associated with the reference configuration $\hat{\mathbf{H}}$. Note that $\mathbf{F}^{(\gamma)}$ provides the mapping from the reference $\hat{\mathbf{H}}$ to the current configuration $\mathbf{H}^{(\gamma)}$. Following this line of thought, we first define the potential energy landscape \mathcal{U} as

$$\mathcal{U}(\mathbf{r}) : \text{conv}(\mathbf{H})^N \rightarrow \mathbb{R}; \mathbf{r} \mapsto \mathcal{U}(\mathbf{r}), \quad (4)$$

depending on the atomic positions \mathbf{r} . In order to keep track of the deformation, we also define the potential energy landscape with respect to the reference configuration as

$$\hat{\mathcal{U}}(\hat{\mathbf{r}}, \gamma) := \mathcal{U}(\mathbf{F}^{(\gamma)} \hat{\mathbf{r}}) : \text{conv}(\hat{\mathbf{H}})^N \times \mathbb{R} \rightarrow \mathbb{R}; \hat{\mathbf{r}} \mapsto \hat{\mathcal{U}}(\hat{\mathbf{r}}, \gamma). \quad (5)$$

Since the configuration remains in a minimum of the potential energy landscape [22, 23, 24], the force, $\hat{\mathbf{f}} \in \mathbb{R}^{dN}$, which is equal to the negative gradient with respect to position, vanishes:

$$\hat{\mathbf{f}}(\hat{\mathbf{r}}, \gamma) := -\nabla_{\hat{\mathbf{r}}} \hat{\mathcal{U}}(\hat{\mathbf{r}}, \gamma) = 0, \quad \text{with} \quad \nabla_{\hat{\mathbf{r}}} := \begin{pmatrix} \frac{\partial}{\partial \hat{\mathbf{r}}_1} \\ \vdots \\ \frac{\partial}{\partial \hat{\mathbf{r}}_{dN}} \end{pmatrix}. \quad (6)$$

Mechanical deformation is induced by altering the Bravais vectors from the reference configuration $\hat{\mathbf{H}}$ to the current configuration $\mathbf{H}^{(\gamma)}$ therefore, also altering the potential energy landscape. However, to ensure mechanical equilibrium, the configuration must remain in a local minimum. Considering that $\hat{\mathbf{f}}$ depends on $\mathbf{H}^{(\gamma)}$, and \mathbf{r} itself depends on $\mathbf{H}^{(\gamma)}$, we evaluate the change in force from the reference to the current configuration as the total derivative:

$$\frac{d\hat{\mathbf{f}}(\hat{\mathbf{r}}, \gamma)}{d\gamma} = -\frac{\partial}{\partial \gamma} \hat{\mathcal{U}}(\hat{\mathbf{r}}, \gamma) + \hat{\mathcal{H}}(\hat{\mathbf{r}}, \gamma) \frac{d\hat{\mathbf{r}}}{d\gamma}, \quad (7)$$

where $\hat{\mathcal{H}}(\hat{\mathbf{r}}, \gamma) = \frac{\partial^2 \hat{\mathcal{U}}(\hat{\mathbf{r}}, \gamma)}{\partial \hat{\mathbf{r}} \partial \hat{\mathbf{r}}}$ refers to the Hessian of the potential energy landscape, depending on both the positions and the shape of the simulation cell. The change in potential energy with respect to the the

cell geometry may be interpreted as a virtual force $\tilde{F} = -\frac{\partial}{\partial \gamma} \hat{\mathcal{U}}(\hat{\mathbf{r}}, \gamma)$ pushing the externally disturbed configuration back into the minimum position. The term $\frac{d\hat{\mathbf{r}}}{d\gamma}$ refers to a change in the reference position due to the external mechanical disturbance, which is a deformation-induced velocity field also referred to as non-affine deformation field [25, 26, 27].

During mechanical deformation, we demand that a change in the force with respect to mechanical deformation is also equal to zero, $\frac{d\tilde{F}(\hat{\mathbf{r}}, \gamma)}{d\gamma} = 0$, leading to the equation of equilibrium for molecular systems:

$$\tilde{F} = \hat{\mathcal{H}}(\hat{\mathbf{r}}, \gamma) \frac{d\hat{\mathbf{r}}}{d\gamma}, \quad (8)$$

which means that an infinitesimally disturbed system experiences a non-affine displacement field $\frac{d\hat{\mathbf{r}}}{d\gamma}$ so that a force \tilde{F} is required to push the system back into its local minimum.

The numerical implementation of the athermal deformation scheme is a finite realization of Equation (7) performed within a two-step process. Figure 1(a,b,c) visualizes the potential energy landscape during one deformation step. Figure 1(a) presents the potential energy landscape belonging to the reference simulation cell. The red ball represents the reference position. In the first step, the configuration \mathbf{H}^0 is externally deformed, inducing small affine increments to $\mathbf{H}^{(\Delta\gamma)}$ and \mathbf{r} using $\mathbf{F}^{(\Delta\gamma)}$, altering the shape of the potential energy landscape. Generally, this leads to the system being pushed out of the local minimum so that we are not in mechanical equilibrium anymore, as indicated in Figure 1(b). In the second step, the shape of the deformed simulation cell $\mathbf{H}^{(\Delta\gamma)}$ is held, while the configuration \mathbf{r} is allowed to relax so that it again falls back into the adjacent local minimum of the potential energy landscape. This relaxation refers to the non-affine portion of the structural response and is realized by minimizing the potential energy landscape. The minimization is formalized as:

$$\mathcal{F}_\gamma : \text{conv}(\mathbf{H}^{(\gamma)})^N \rightarrow \text{conv}(\mathbf{H}^{(\gamma)})^N, \quad (9)$$

$$\mathbf{r} \mapsto \Omega_{\mathbf{r}, \gamma} := \left\{ \mathbf{r}_\infty = \lim_{t \rightarrow \infty} \mathbf{r}(t) \mid \frac{d}{dt} \mathbf{r}(t) = -\nabla_{\mathbf{r}} \mathcal{U}(\mathbf{r}(t)); \mathbf{r}(0) = \mathbf{r} \right\},$$

which is the limit of the gradient flow and ends up in the adjacent local minima (assuming the gradient does not vanish for \mathbf{r}). Generally we use a conjugate gradient method with \mathbf{r} as the initial guess.

For ease of notation, we also use the iterated concatenation, i.e.

$$\left(\mathcal{F}_\gamma \circ \mathbf{F}^{(\Delta\gamma)} \right)^n (\mathbf{r}) := \mathcal{F}_\gamma \left(\mathbf{F}^{(\Delta\gamma)} \left(\mathcal{F}_\gamma \left(\mathbf{F}^{(\Delta\gamma)} \left(\dots \mathbf{F}^{(\Delta\gamma)} (\mathbf{r}) \dots \right) \right) \right) \right). \quad (10)$$

Using that notation, we combine the two steps into a single AQS step $\mathcal{F}_\gamma \circ \mathbf{F}^{(\Delta\gamma)}$, and repeating them in a sequence results in the athermal quasistatic deformation protocol:

$$\mathbf{r}_k := (\mathcal{F}_\gamma \circ \mathbf{F}^{(\Delta\gamma)})(\mathbf{r}_{k-1}) = (\mathcal{F}_\gamma \circ \mathbf{F}^{(\Delta\gamma)})^k(\mathbf{r}_0), \quad (11)$$

where \mathbf{r}_k is the particle configuration in the respective local minimum of the potential energy landscape after k deformation steps which is confined in the space $\text{conv}(\mathbf{H}^{(\gamma)})^N$ for $\gamma = k\Delta\gamma$. Per construction the deformation happens in equidistant steps of $\Delta\gamma$.

We define the intermediate step $\tilde{\mathbf{r}}_k$ as the athermal disturbance induced by $\mathbf{F}^{(\Delta\gamma)}$:

$$\tilde{\mathbf{r}}_k := \mathbf{F}^{(\Delta\gamma)}(\mathbf{r}_{k-1}) = \left(\mathbf{F}^{(\Delta\gamma)} \circ (\mathcal{F}_\gamma \circ \mathbf{F}^{(\Delta\gamma)})^{k-1} \right)(\mathbf{r}_0). \quad (12)$$

To calculate the configuration at deformation step k , \mathbf{r}_k , one must follow the sequence of $k-1$ times the affine mapping followed by the non-affine correction, as shown in Figure 1(d). Also, here, the configuration is indicated by the red ball. It runs along a path of local minima in the potential energy landscape, which gradually changes its shape after every deformation step. Since we are looking for adjacent minima, line search algorithms, such as the steepest descent or conjugate gradient method, have proven effective in this regard. Because of its superior efficiency, we chose to use the conjugate gradient method for this task.

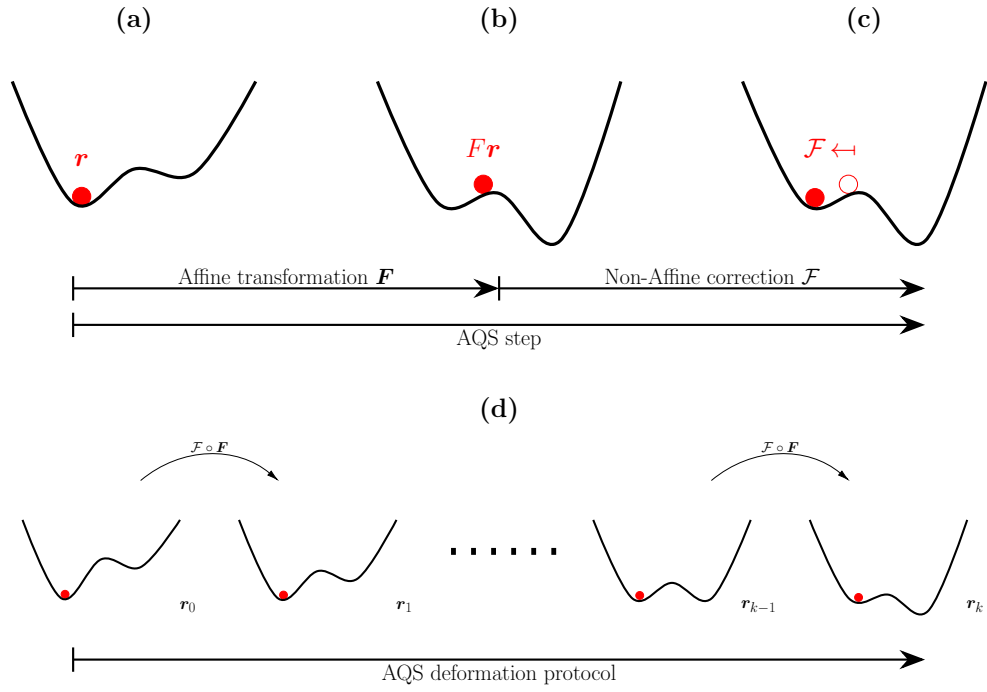


Figure 1: Illustration of the athermal quasistatic deformation on a one-dimensional potential energy landscape; (a) undeformed configuration; (b) configuration after affine displacement mapping; (c) non-affine correction; (d) and entire athermal deformation protocol of k steps.

2.1. The benchmark problem

To demonstrate our procedure, we present the mechanical response of a binary Lennard-Jones glass [28, 29] to simple shear deformation. Glasses exhibit highly complex response behavior to mechanical deformation due to their inherently disordered structure, making response evaluation numerically challenging as it relies on fine local geometrical details in the atomic structure.

The Lennard Jones interatomic pair potential [30] is written as:

$$U(r_{ij}) = 4\epsilon \left[\left(\frac{\sigma}{r_{ij}} \right)^{12} - \left(\frac{\sigma}{r_{ij}} \right)^6 \right], \quad (13)$$

with σ referring to the zero energy distances and ϵ quantifying the bond strength. The system consists of two different particle types, the small particle type (S) and the large particle type (L). The three zero-energy distance parameters are defined as:

$$\sigma_{SS} = 2 \sin \left(\frac{\pi}{10} \right), \quad \sigma_{LL} = 2 \sin \left(\frac{\pi}{5} \right), \quad \sigma_{SL} = 1. \quad (14)$$

The three bond strength parameters are defined as:

$$\epsilon_{SS} = \frac{1}{2}, \quad \epsilon_{LL} = 1, \quad \epsilon_{SL} = \frac{1}{2}. \quad (15)$$

We used Lennard-Jones units, and all output quantities depending on the potential are normalized with respect to a maximum value.

To rigorously test the new approach presented in this paper on a set of 10^3 material samples, generated using the melting quenching technique [31, 32]. This way, we first position 400 atoms in a two-dimensional simulation cell. The length of the cell is chosen so that the material has an average density of one particle per \AA^2 , leading to quadratic cell sizes with a side length of 20 \AA in the initial configuration. The initial position is geometrically ordered, but the type of particle is random. This ensures physically possible states, prohibiting individual positions of the particles from being, by chance, too close. The ratio between large and small particles is chosen as the golden mean, that is, $\frac{N_L}{N_S} = \frac{1+\sqrt{5}}{4}$ [33]. Melting quenching is performed within an NVT-ensemble [31, 34, 4, 35], where the number N of particles, the volume V , and the temperature T stay constant. This way, the $2N$ -dimensional system is extended by an additional degree of freedom ξ , which allows for controlling the temperature of the system by manipulating the mean velocity of particles, acting as a thermostat to the ensemble [31, 36, 37, 38]. The extended equations of motion were solved using the Velocity Verlet algorithm [11]. The system was equilibrated for one million time integration steps above the melting temperature, using a step size of 0.005 femtoseconds to ensure that no correlation between the initial and the equilibrated configuration was present. Starting from this equilibrated glass melt, we further equilibrated the system for 10^8 steps, keeping the temperature constant and saving a total number of 10^3 melted samples in equidistant time intervals of 10^6 integration steps. After that, every saved melted configuration was quenched for 10^6 steps to 0.001 Kelvin, allowing the system to approach a local minimum of the potential energy landscape. Finally, the conjugate gradient algorithm was performed to position the atomic structures precisely within the local basin of the potential energy landscape. This procedure results in 10^3 uncorrelated, relaxed samples at zero temperature. One such sample is shown in Figure 2(a). During the shearing process, meaningful information can be seen when the structure's potential energy and total stress are considered, as seen in Figure 5.

Having generated the set of 10^3 test samples, we subjected the configurations to athermal simple shear deformation protocols. The simple shear mapping during deformation increment $\Delta\gamma$ from the reference to the current configuration $\mathbf{F}^{(\Delta\gamma)}$ is written as:

$$\mathbf{F}^{(\Delta\gamma)} = \begin{pmatrix} 1 & \Delta\gamma \\ 0 & 1 \end{pmatrix} \in \mathbb{R}^{d \times d}. \quad (16)$$

Notably, the Bravais tensor is subjected to the simple shear mapping, while the particle configurations are subjected to the mapping $(\mathbf{F}^{(\Delta\gamma)})^N$ from (3).

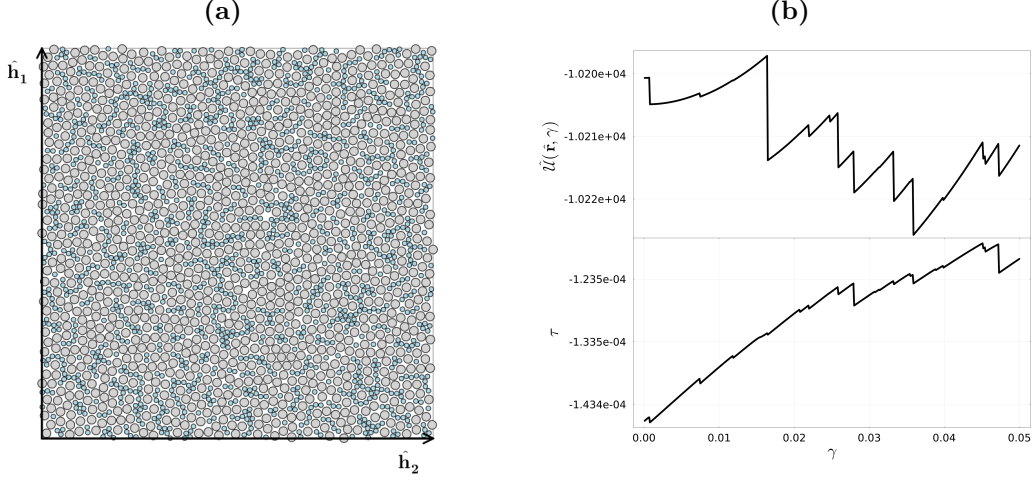


Figure 2: The binary Lennard-Jones glass subjected to an athermal simple shear deformation protocol; (a) One out of 10^3 material samples; (b) Potential energy $\tilde{U}(\tilde{\mathbf{r}}, \gamma)$, versus shear strain γ and the corresponding stress-strain response $\tau := \sigma_{12}$ versus shear strain γ .

3. Parallel athermal stepping

3.1. Ansatz

By definition, every iteration during one deformation step in the procedure, as defined by Equation (11), depends on the previous increment. As a consequence, before calculating the configuration \mathbf{r}_k , one needs to solve the dN -dimensional optimization problem $k - 1$ times successively. This can be extremely slow, as the deformation increments must be sufficiently small to resolve all drops in the potential energy landscape.

In the following, we present an approach, inspired by the *Parareal* Algorithm [39] for differential equations, offering a parallel computing scheme by adapting it to our case. In general, the procedure starting configurations by performing a small sequence of coarse steps, which we refer to as level I stepping. We introduce a coarse step size $\Delta\gamma^c = K\Delta\gamma$ for some $K \in \mathbb{N}_{>1}$, which in turn defines a new affine displacement matrix $\mathbf{F}^{(\Delta\gamma^c)}$, as shown in Equation (16). This step size implies a course intermediate step as

$$\mathbf{r}_K^c := \mathbf{F}^{(\Delta\gamma^c)} \mathbf{r}_0 \quad (17)$$

Level I stepping utilizes exclusively affine projection. Thus, after applying this coarse transformation $P - 1$ times, no minimization is performed, thus, visiting configurations that are not located in minima of the potential energy landscape. In the setting $P \in \mathbb{N}_{>1}$ is the number of equally capable threads (processors) available. Notably, this sequence of affine mappings is computationally insignificant since these mappings are realized by ordinary matrix multiplication. This level I procedure provides a set of initial configurations, each of which serves as a starting point for further processing. Then, every coarse level I increment is assigned to one individual calculation thread, which we refer to as level II stepping. Every thread at level II stepping then performs athermal quasistatic deformation increments individually, proposing a sequence of equilibrium candidates. Starting from different intermediate results may affect the final configuration of the procedure since the potential energy landscape is highly non-convex. Therefore, starting at a particular level I initial configuration and performing K level II fine AQS steps, one ends up at a macroscopic state that corresponds to the same shear as the subsequent level I coarse configuration. However, the local minimum at the subsequent level I coarse step may not be the same minimum we find after performing the number of K level II fine steps. In this case, coarse level I stepping went along the wrong deformation path. In order to keep track of such possibilities, we introduce the following conditional notation:

$$\mathbf{r}_{k_2} | \mathbf{r}_K^c := (\mathcal{F}_\gamma \circ \mathbf{F}^{(\Delta\gamma)})^{k_2-K} (\mathbf{r}_K^c) = \left((\mathcal{F}_\gamma \circ \mathbf{F}^{(\Delta\gamma)})^{k_2-K} \circ \mathbf{F}^{(\Delta\gamma^c)} \right) (\mathbf{r}_0). \quad (18)$$

Note that indexing of the coarse steps is in absolute terms, meaning one coarse step moves the index by K , e.g., $\mathbf{r}_K^c = (\mathbf{F}^{(\Delta\gamma^c)})(\mathbf{r}_0)$. In the following, we introduce the implementation of the parallel stepping scheme taking into account the correction of possible miss-predictions during level I stepping.

3.2. Calculation scheme

Given an initial minimum in the potential energy landscape as our starting configuration, \mathbf{r}_0 , we calculate a set of $P - 1$ coarse steps

$$\{\mathbf{r}_0, \mathbf{r}_K^c, \dots, \mathbf{r}_{(P-2)K}^c, \mathbf{r}_{(P-1)K}^c\},$$

which could also be done in parallel; however, one such step only requires a dN -dimensional matrix multiplication since no minimization is performed. Then, we apply the operation $(\mathcal{F}_\gamma \circ \mathbf{F}^{(\Delta\gamma)})^K(\mathbf{r})$, while \mathbf{r} is taken from the set of the level I coarse configurations.

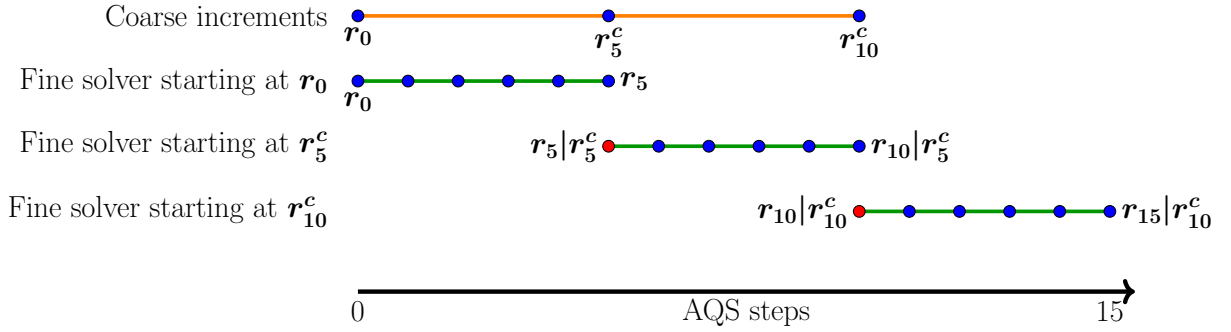


Figure 3: Scheme of parallel computing approach. The first row is calculated sequentially, while the other three rows are done in parallel.

For the following, we note that one macroscopic strain state, indexed by \hat{k} , may have multiple equilibrium states as potential solution candidates, i.e. there exist multiple local basins in the PES for any given strain state. Therefore, we now define \hat{k} as strain states, for which we calculated multiple configurations, called node states. The node set $S_{\hat{k}}$ contains the incoming configuration $\mathbf{r}_{\hat{k}}|\mathbf{r}_{\hat{k}-K}^c$, coarse configuration $\mathbf{r}_{\hat{k}}^c$ and the outgoing configuration $\mathbf{r}_{\hat{k}}|\mathbf{r}_{\hat{k}}^c$. Let's take a look at the node state $\hat{k} = 5$ in Figure 3, where we schematically perform a 15-step AQS procedure applying parallel athermal stepping. Using three processors for 15 steps in total, one defines three level I coarse starting configurations $\{\mathbf{r}_0, \mathbf{r}_5^c, \mathbf{r}_{10}^c\}$. This way, one initiates three individual level II AQS stepping schemes on three processors, simultaneously starting from \mathbf{r}_0 , \mathbf{r}_5^c , and \mathbf{r}_{10}^c respectively. After this, the first set of solution candidates for the AQS response trajectory is set up to step 15. We now define incoming configurations as \mathbf{r}_5 and $\mathbf{r}_{10}|\mathbf{r}_5^c$ and outgoing configurations as $\mathbf{r}_5|\mathbf{r}_5^c$ and $\mathbf{r}_{10}|\mathbf{r}_{10}^c$ for the node states 5 and 10, respectively. Notably $\mathbf{r}_5|\mathbf{r}_5^c$ and $\mathbf{r}_{10}|\mathbf{r}_{10}^c$ are the results of the minimization operation \mathcal{F}_γ on \mathbf{r}_5^c and on \mathbf{r}_{10}^c , respectively. In the following, we check the validity of the solution candidates and correct them if necessary. The method is also summarized in Algorithm 0.

3.3. Equality and concatenation of configurations

In the respective node states (strain states), the outgoing and incoming configurations are now compared for equality for increasing index k to determine if our possible candidates can be accepted as the correct configurations. If the incoming and outgoing configurations are identical, the solutions can be concatenated. If this is not the case, the entire potential solution trajectory after this state onward must be rejected. For our example in Figure 3 this means that, if \mathbf{r}_5 and $\mathbf{r}_5|\mathbf{r}_5^c$ are equal, then we assume that the solution $\mathbf{r}_{10}|\mathbf{r}_5^c$ is also correct, however, if \mathbf{r}_5 and $\mathbf{r}_5|\mathbf{r}_5^c$ are not equal we must initiate the procedure again starting from \mathbf{r}_5 , while rejecting all upcoming configurations. To precisely define the concept of equality in this case, we

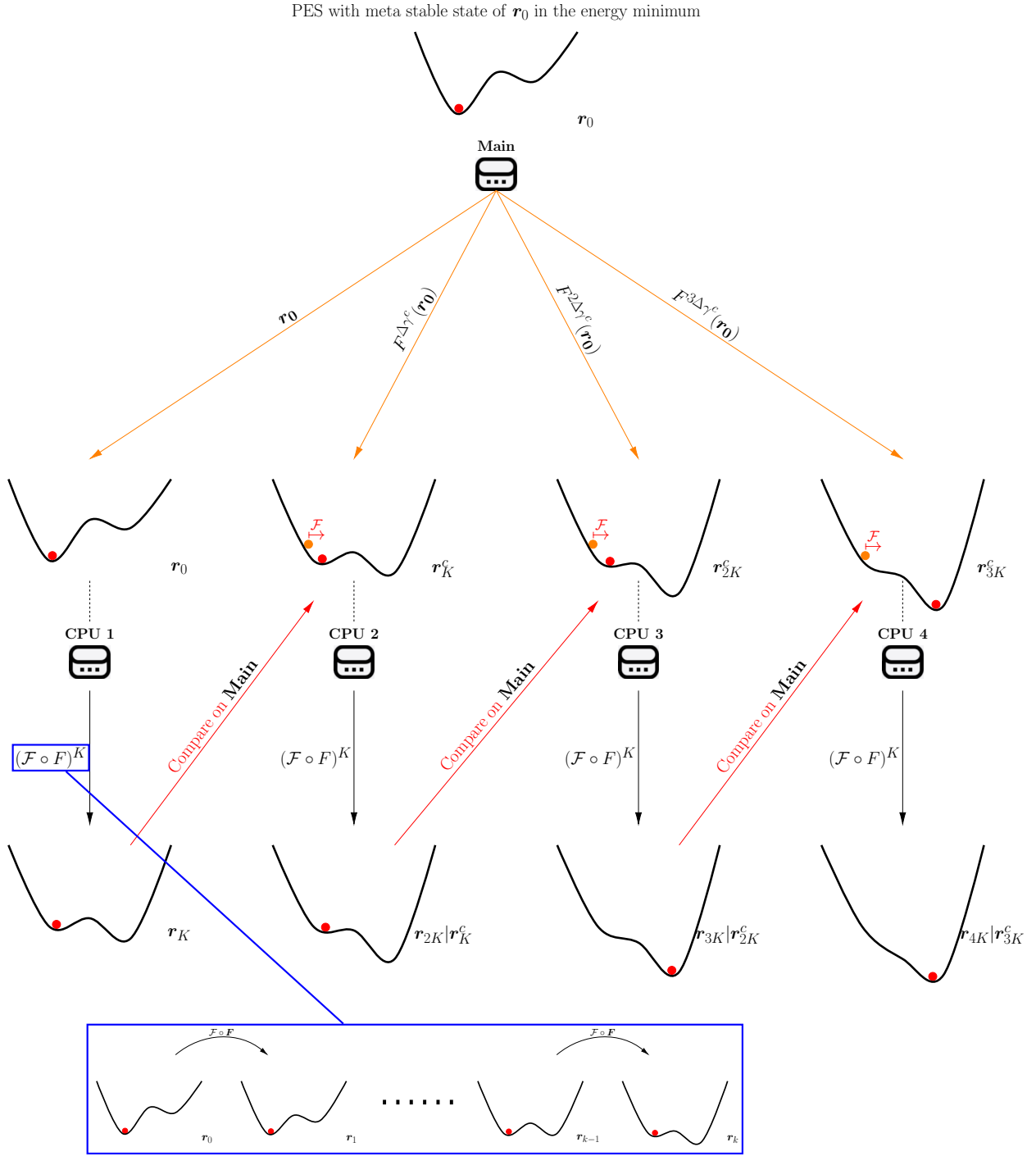


Figure 4: Scheme of parallel computing approach. The intermediate steps are distributed to the different processors on which the fine steps are calculated. On every processor a K -step AQS procedure is simulated as illustrated with Figure 1(d) in the blue box.

introduce the following concept. Two configurations $\mathbf{r}_a, \mathbf{r}_b \in \text{conv}(\mathbf{H}^{(\gamma)})^N$ are equal if and only if they are within the same local minima, i.e., basin of attraction defined in (9),

$$\mathbf{r}_a = \mathbf{r}_b \quad \Leftrightarrow \quad \Omega_{\mathbf{r}_a, \gamma} = \Omega_{\mathbf{r}_b, \gamma} . \quad (19)$$

A configuration \mathbf{r}_i is considered correct if

1. it originates from a correct configuration \mathbf{r}_j , meaning an arbitrary number z of fine steps are performed in between, i.e., $\mathbf{r}_i = (\mathcal{F}_\gamma \circ \mathbf{F}^{(\Delta\gamma)})^z(\mathbf{r}_j)$.
2. $\mathbf{r}_i | \mathbf{r}_i^c$ is an outgoing configuration which is equal, in the sense of definition (19), to the incoming configuration $\mathbf{r}_i | \mathbf{r}_{i-K}^c$.

Using the definition of a correct configuration, one needs to check the $P - 2$ node sets in ascending order

$$S_K, \dots, S_{(P-1)K} ,$$

stepping through the node states within the entire deformation protocol. In Figure 5, we provide an exemplary parallel athermal stepping scheme. One can see that the newly established scheme can work in parallel, successfully reducing the total computational time.

Algorithm 1 Parallel procedure

```

1: procedure AQS_PARALLEL( $\mathbf{r}_0, \hat{\mathbf{H}}, \mathbf{F}^{(\Delta\gamma)}, \Delta\gamma, N_{steps}, K, P$ )
2:    $N_{current} \leftarrow 0$ 
3:    $\mathbf{r}_\star \leftarrow \mathbf{r}_0$ 
4:   while  $N_{current} < N_{steps}$  do
5:     Lvl I steps:  $L \leftarrow [(\mathbf{F}^{(k\Delta\gamma^c)}) \mathbf{r}_\star \text{ for } k = 0, \dots, P-1]$ 
6:     for  $i = 1$  to  $P$  do
7:       Lvl 2 steps:  $M_i \leftarrow (\mathcal{F}_\gamma \circ \mathbf{F}^{(\Delta\gamma)})^K(L_i)$ 
8:     end for
9:      $S = \{S_K, \dots, S_{(P-1)K}\} \leftarrow \text{create\_node\_sets}(L, M)$ 
10:     $\mathbf{r}_\star \leftarrow \text{compare}(S)$ 
11:     $N_{current} \leftarrow \text{update\_count}(\mathbf{r}_\star)$ 
12:  end while
13: end procedure

```

3.4. Response trajectories in the potential energy landscape

In the following, we will break down parallel athermal deformation stepping with the help of the visualization of the evolution of a one-dimensional potential energy landscape varying over the shear strain γ , shown in Figure 6. In this figure, the evolution of local minima is presented by black dashed lines, while the evolution of local maxima is presented by continuous black lines. This illustrative example reveals four maxima, referred to as A, B, C , and D , and four minima, referred to as 1, 2, 3, and 4. Our solution trajectory candidates lie on local minimum energy paths. Minimum and maximum energy paths may merge into saddle points when increasing the shear strain, where the configuration jumps from one to an adjacent equilibrium state. In Figure 6, we see one saddle node when maximum B and minimum 2 merge and another saddle node when maximum D and minimum 3 merge. With increasing strain, the curvature gradually decreases, which can be quantified by the lowest eigenvalue of the Hessian of the potential energy landscape, until the minimum merges into the saddle node, the system becomes unstable. During such an event, the potential energy drops, leading to a sudden finite change in the configurational coordinate \mathbf{r} . In the configuration space, such events are localized sudden atomic-scale rearrangements while the surrounding material responds elastically, often also referred to as shear transformations [40]. Let us assume now that a minimum of 3 is the correct value at zero shear strain and proceed with the exploration from there. A conventional step-by-step AQS protocol is presented in green in Figure 6. Proceeding in finite strain increments, one macroscopically

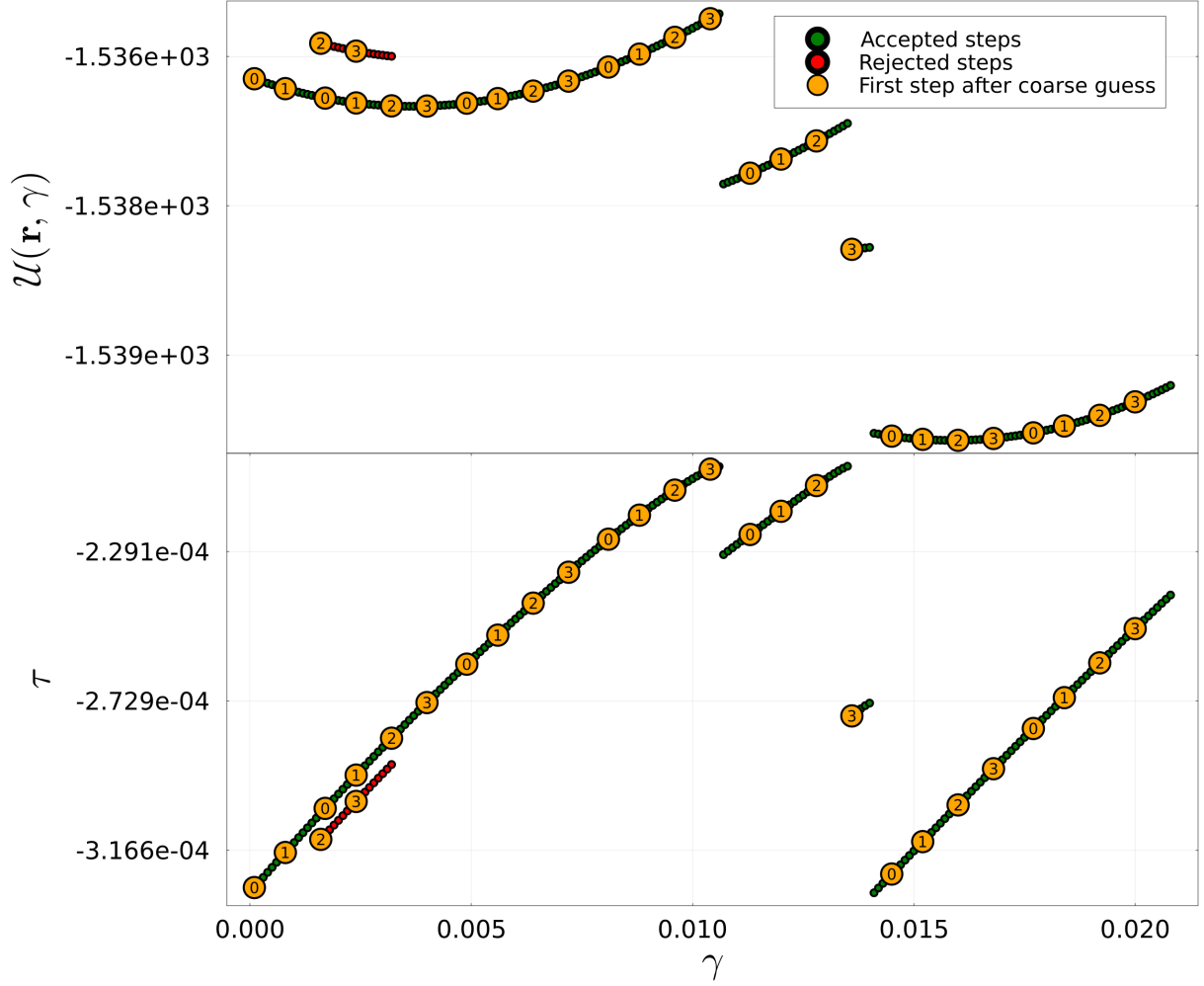


Figure 5: Example AQS simulation in parallel scheme for $P = 4$ and a total of 200 steps with $\Delta\gamma = \frac{1}{200}$. On each processor, $K = 8$ fine steps were performed per iteration. The orange dots represent the node points, each is marked with the processor index. If the following *outgoing configuration* is equal, the steps are accepted and the points are colored in green. If a configuration is not accepted at the node, the configurations that follow are colored red.

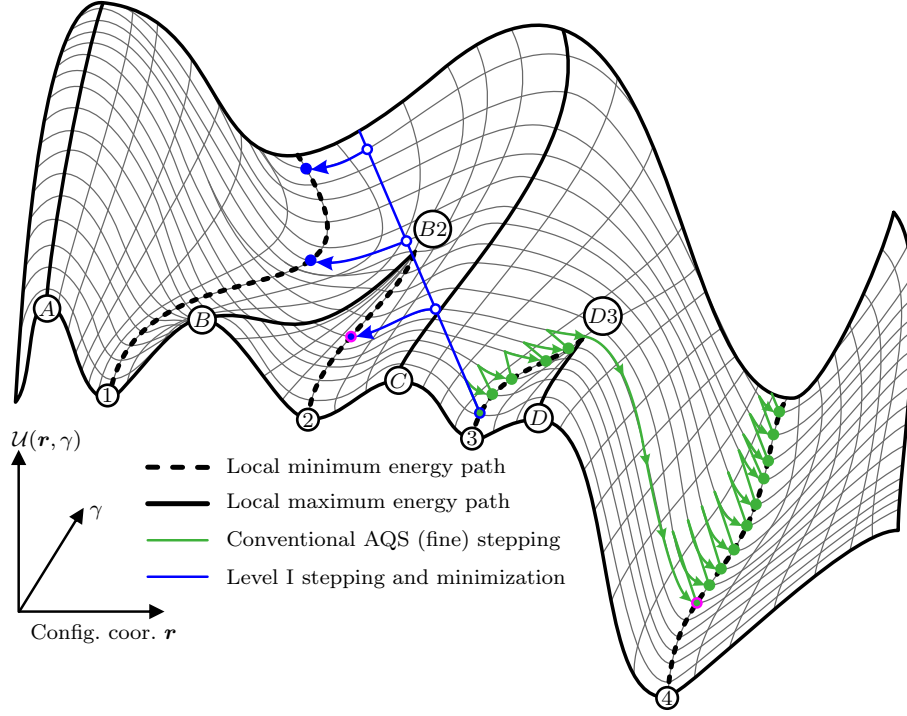


Figure 6: Evolution of a one-dimensional potential energy landscape with increasing shear deformation.

deforms the system and pushes the configuration out of minimum 3. Every minimization step pushes the system back into the minimum configuration while the shear strain is fixed. The system is further driven to the saddle node $D3$ and drops down into the adjacent minimum 4, where the system is further driven by external shear. The coarse level I stepping is represented in blue in Figure 6. Here, we show a scenario in which the parallel stepping scheme will lead to an incorrect response trajectory and will be rejected. One starts at the same point and pushes the system into the same affine direction as the conventional stepping scheme. We remind that level I stepping is a sequence of exclusively affine mappings, which means we receive the intermediate deformation states indicated by the white markers on an extension of the same line. We see that, performing a larger stepping length, the configuration is pushed across the maximum energy path C already after the first affine mapping, and it remains on the other side of the local maximum energy path C . However, one does not know that as long as one does not evaluate the corresponding inherent states by performing minimization of the potential energy landscape. As more elaborately discussed in Sections 3.1, 3.2 and 3.3, we perform now level II stepping, which consists of initiating multiple AQS sequences of fine stepping from the configurations indicated by the blue markers in Figure 6. Notably, one starting point is located on one side of the local maximum energy path C while the other three starting points are located on the other side of C . However, only after checking different states at the same macroscopic strain for equality according to Section 3.3, we can reject the level I proposals. Considering the special case in Figure 6, the incoming configuration is indicated in magenta in the local minimum energy path 4 while the corresponding outgoing configuration is indicated in magenta in the local minimum energy path 2. Consequently, all strain states after the magenta configurations are not considered further, and new level I proposals are set from there. We note that the solution trajectory of athermal stepping is numerically equivalent to the one obtained by performing conventional AQS deformation stepping. However, what we generally observe when performing parallel stepping is the possibility of getting trapped in alternative solution paths, eventually leading to rejections and recalculations. This occurs when the level one stepping crosses local maxima and explores new basins in the potential energy landscape. It should be noted that, since the problem is highly nonlinear in its nature, proceeding along an alternative minimum energy path without rejection could lead

to an entirely different macroscopic failure picture in the material.

Athermal stepping is purely deterministic. Thus, repeating one simulation will result in exactly the same outcome. However, this is not the case when including temperatures. Thus, from a molecular dynamics perspective, hopping over a maximum energy path, such as path C in Figure 6, is a scenario that might occur during thermal deformation since thermal vibration may result in the system falling into the minimum energy path 2. Clearly, the probability of this happening depends largely on the activation energy necessary to reach the maximum energy point in C and the height of the opposite maximum energy point D . Therefore, although proceeding along path 1 in Figure 6 is strictly speaking incorrect from a mathematical perspective, it may constitute a physically meaningful response trajectory and might be valuable for investigations at finite temperature.

4. Results

All 1000 samples have been deformed using the standard AQS method and the new parallel stepping scheme. For all samples, the same computer architecture and hyperparameters $K, \Delta\gamma$, were used, while changing the number of processors P . Considering one sample i , let the machine time be $C_i^{(S)}$ for the standard method and $C_i^{(p)}$ using $p \in \{4, 8, 16, 32\}$ the computing time for the parallel stepping method. We quantified the speed up as:

$$S_{i,p} = \frac{C_i^{(S)}}{C_i^{(p)}}. \quad (20)$$

The results of the achieved speed up can be seen in Figure 7, where $\{S_{i,p}\}_{i \in \{1, \dots, 1000\}}^{p \in \{4, 8, 16, 32\}}$ is represented in a histogram. In all cases, we observed a considerable advantage when using the parallel stepping scheme.

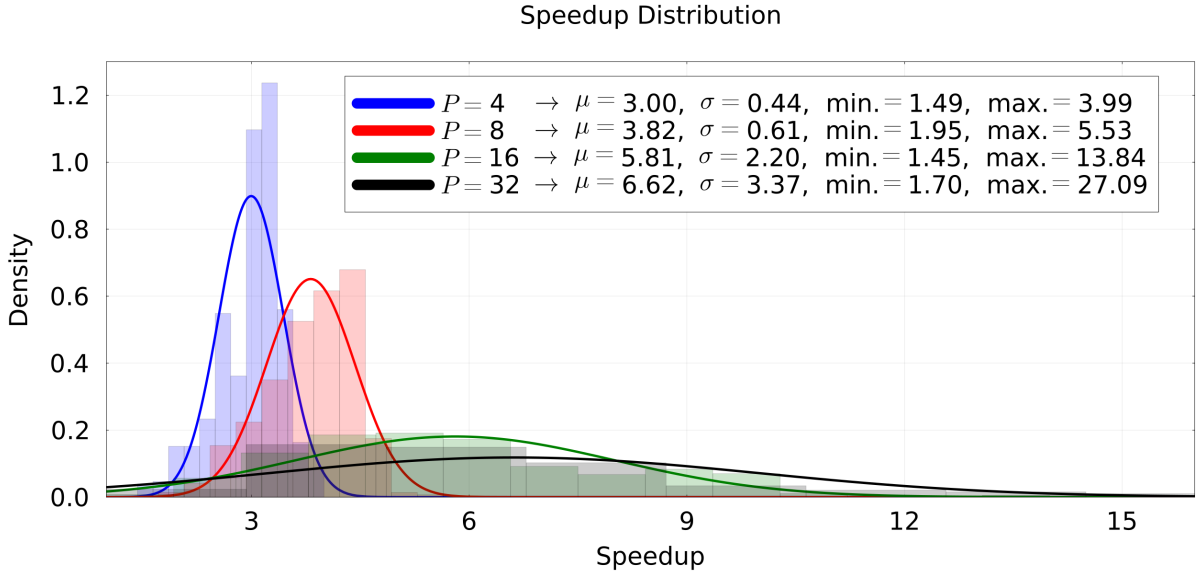


Figure 7: Distribution of speed up for different samples. The same initial parameters of $K = 8, \Delta\gamma = \frac{1}{200}$ and 200 total steps were used for all 1000 samples.

Notably, all results were equal in the sense defined in Section 3.3 when considering the final configuration for both methods per sample. The average speed up observed was 200, 282, 481, 562% for $P = 4, 8, 16, 32$ respectively, while the lower bound was 45%. We emphasize that all speed-ups come without any loss in numerical or approximation accuracy. In the worst scenario, that is, if every level I projection needs to be rejected, the parallel stepping scheme is as fast as the conventional athermal quasistatic deformation

protocol on a single processor. However, as also shown in Figure 7, this scenario never occurred during 1000 sample runs.

4.1. Scaling and hyper-parameters

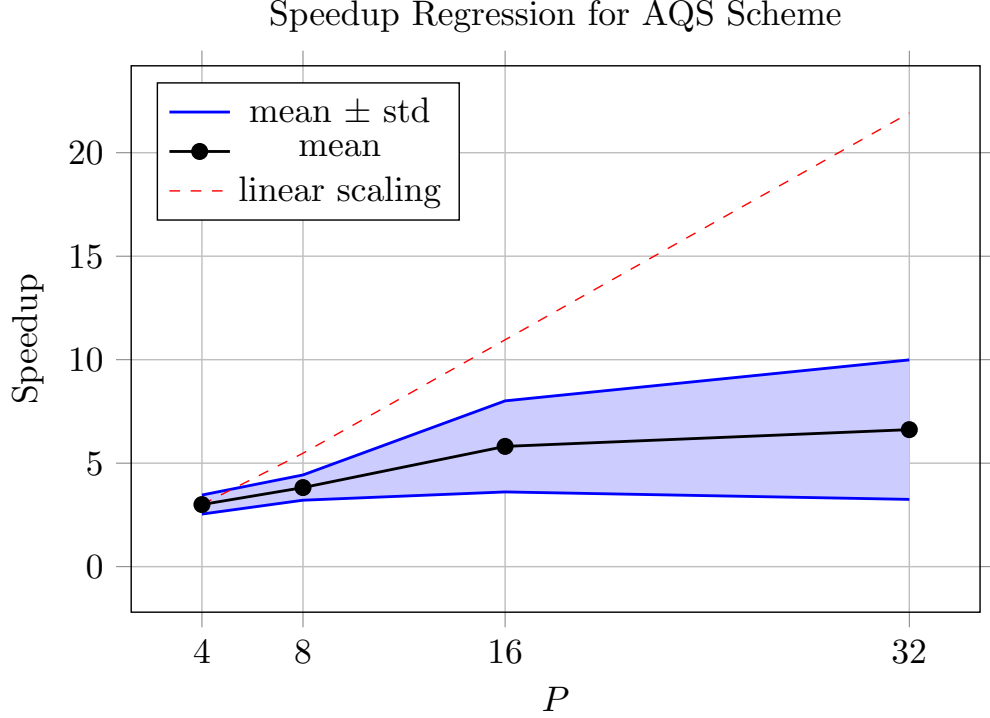


Figure 8: Speed up relative to the number of processors P .

As this method uses P processors at the same time it is important to note, that the average and maximum speed up do not scale linear w.r.t. P . This is because when using P processors we ask of each processors to do the operation $(\mathcal{F}_\gamma \circ \mathbf{F}^{(\Delta\gamma)})^K$ and in a perfect world each of the processor takes the same amount of time and comes back to the main processor, as in Figure 4 at the same time. However, each operation \mathcal{F}_γ takes an a-priori unknown number of CG minimization steps, which is the main contributor to compute time on a isolated processor. In consequence this means all processors need to wait for the processor taking the most amount of time, equivalently the one with greatest number of total CG steps in the K minimization procedures. The other factor of losing efficiency with growing number of processor is the increased likelihood of miss-predictions. Those phenomena are visible in Figure 8, where we can see that doubling P leads to higher average speed-up but will also increase the observed standard deviation. It is important to note, that the number K was kept constant. An increasing number P also increases the chances of miss-predictions meaning following result suggestions must be rejected, this is also the reason for increase in standard deviation. The most efficient set of hyperparameters is not known a-priori for any problem, meaning one must currently use educated guessing.

4.2. Reproducibility

All of the numerical work was done in the Julia programming language [41] and is available in the open source GitHub repository **Jumol** [42]. The code is open source, and we invite everyone interested to contribute.

5. Conclusion and future work

In this paper, we presented a parallel athermal stepping scheme offering a significant numerical speed-up without any loss in solution accuracy.

Our method builds on the concept that performing multiple AQS runs at the same time, individually connecting configurations at different strain states, allows for a parallelization of the deformation procedure. This is by exploiting the mostly moderate change of the potential energy landscape with increasing strain. The verification process ensures that the landscape has not had any plastic or erratic changes, and the correct response trajectory is found. We show that this method provides indeed significant speed-ups of at most a factor of P when compared to the conventional AQS method, however this does not scale linearly with the number of processors P as discussed and observed in Figure 8. However, the aim of the algorithm is to consistently lower computational time when multiple processors are available. This is done without any sacrifice in terms of accuracy compared to the same strain step size $\Delta\gamma$ of the standard AQS protocol. The negligible overhead cost lowers the bounds of the parallel method by the standard AQS protocol. Our proposed method can be applied to a wide range of molecular systems to investigate inelastic deformation and fracture. Although we provided numerical benchmark examples investigating exclusively shear behavior of complex materials, the method can be easily extended to more general deformations as well as more complex deformation histories, such as cyclic deformation protocols. Furthermore, the parallel stepping scheme provides a basis for a framework that efficiently finds multiple sets of alternative solution trajectories. Such alternative paths in the potential energy landscape are not relevant when performing athermal overdamped simulations but might be visited when performing molecular simulations at finite temperatures. This way, further steps should be to develop numerically efficient strategies for finite temperature deformation, where the final material response trajectory is a result of probabilistic considerations taking into account a set of multiple trajectory candidates.

In future research, it is desirable to find ways to a-priori prevent miss-predictions in order to reliably achieve a speed-up of close to the factor P . A dynamical step-sizing would possibly be able to use a large number of processors P , which are available through high-performance clusters, for this the parameter K must also be taken into account dynamically. Future work will also involve developing extrapolation methods for the standard AQS protocol to minimize the number of steps in the minimization procedure. This can also be used on each of the parallel processors, thereby speeding up both the parallel stepping method and the standard AQS method.

CRedit authorship contribution statement

Maximilian Reihn: Writing - review & editing, Writing - original draft, Numerical work, Methodology; **Franz Bamer:** Writing - review & editing, Writing - original draft, Numerical Work; **Benjamin Stamm:** Review & editing, Methodology.

Data availability

No data was used for the research described in the article. The code used is publicly available.

Declaration of interests

The authors declare that they have no known competing financial interests or personal relationships that could have appeared to influence the work reported in this paper.

Acknowledgment

The authors acknowledge financial support by the Deutsche Forschungsgemeinschaft (DFG) under project number 523939420.

References

- [1] A. Rapaport, A. Maloum, Design of exponential observers for nonlinear systems by embedding, *International Journal of Robust and Nonlinear Control* 14 (3) (2004) 273–288. doi:<https://doi.org/10.1002/rnc.878>.
- [2] H. Dal, O. Gültekin, S. Başdemir, A. K. Açıkan, Ductile–brittle failure of amorphous glassy polymers: A phase-field approach, *Computer Methods in Applied Mechanics and Engineering* 401 (2022) 115639. doi:<https://doi.org/10.1016/j.cma.2022.115639>.
URL <https://www.sciencedirect.com/science/article/pii/S0045782522005941>
- [3] D. Raabe, *Computational Materials Science: The simulation of materials. Microstructures and properties.*, WILEY-VCH, 1998.
- [4] S. Nosé, A unified formulation of the constant temperature molecular dynamics methods, *Journal of Chemical Physics* 81 (1984) 511–519.
URL <https://api.semanticscholar.org/CorpusID:5927579>
- [5] H. C. Andersen, Molecular dynamics simulations at constant pressure and/or temperature, *Journal of Chemical Physics* 72 (1980) 2384–2393.
URL <https://api.semanticscholar.org/CorpusID:34820304>
- [6] M. Dobson, I. Fox, A. Saracino, Cell list algorithms for nonequilibrium molecular dynamics, *Journal of Computational Physics* 315 (2016) 211–220. doi:<https://doi.org/10.1016/j.jcp.2016.03.056>.
URL <https://www.sciencedirect.com/science/article/pii/S0021999116300213>
- [7] S. Plimpton, Fast parallel algorithms for short-range molecular dynamics, *Journal of Computational Physics* 117 (1) (1995) 1–19. doi:<https://doi.org/10.1006/jcph.1995.1039>.
- [8] J. Tranchida, S. Plimpton, P. Thibaudau, A. Thompson, Massively parallel symplectic algorithm for coupled magnetic spin dynamics and molecular dynamics, *Journal of Computational Physics* 372 (2018) 406–425. doi:<https://doi.org/10.1016/j.jcp.2018.06.042>.
URL <https://www.sciencedirect.com/science/article/pii/S0021999118304200>
- [9] S. J. Plimpton, Fast parallel algorithms for short-range molecular dynamics, *Journal of Computational Physics* 117 (1993) 1–19.
URL <https://api.semanticscholar.org/CorpusID:15881414>
- [10] J. C. Phillips, R. Braun, W. Wang, J. C. Gumbart, E. Tajkhorshid, E. Villa, C. Chipot, R. D. Skeel, L. V. Kalé, K. Schulten, Scalable molecular dynamics with namd, *Journal of Computational Chemistry* 26 (2005).
URL <https://api.semanticscholar.org/CorpusID:13940583>
- [11] L. Verlet, Computer "experiments" on classical fluids. i. thermodynamical properties of lennard-jones molecules, *Phys. Rev.* 159 (1967) 98–103. doi:[10.1103/PhysRev.159.98](https://doi.org/10.1103/PhysRev.159.98).
URL <https://link.aps.org/doi/10.1103/PhysRev.159.98>
- [12] H. Grubmüller, H. Heller, A. Windemuth, K. Schulten, Generalized verlet algorithm for efficient molecular dynamics simulations with long-range interactions, *Molecular Simulation* 6 (1991) 121–142.
URL <https://api.semanticscholar.org/CorpusID:30391407>
- [13] D. Fincham, Choice of timestep in molecular dynamics simulation, *Computer Physics Communications* 40 (2) (1986) 263–269. doi:[https://doi.org/10.1016/0010-4655\(86\)90113-X](https://doi.org/10.1016/0010-4655(86)90113-X).
- [14] F. Ormeño, I. J. General, Convergence and equilibrium in molecular dynamics simulations, *Communications Chemistry* 7 (1) (2024) 26. doi:<https://doi.org/10.1038/s42004-024-01114-5>.
- [15] M. L. Falk, C. E. Maloney, Simulating the mechanical response of amorphous solids using atomistic methods, *The European Physical Journal B* 75 (4) (2010) 405–413.
- [16] T. C. Hufnagel, C. A. Schuh, M. L. Falk, Deformation of metallic glasses: Recent developments in theory, simulations, and experiments, *Acta Materialia* 109 (2016) 375–393. doi:<https://doi.org/10.1016/j.actamat.2016.01.049>.
URL <https://www.sciencedirect.com/science/article/pii/S1359645416300465>
- [17] K. Muralidharan, K.-D. Oh, P. A. Deymier, K. Runge, J. H. Simmons, Molecular dynamics simulations of atomic-level brittle fracture mechanisms in amorphous silica, *Journal of Materials Science* 42 (2007) 4159–4169. doi:<https://doi.org/10.1007/s10853-007-1638-2>.
- [18] M. L. Falk, J. S. Langer, Dynamics of viscoplastic deformation in amorphous solids, *Phys. Rev. E* 57 (1998) 7192–7205. doi:[10.1103/PhysRevE.57.7192](https://doi.org/10.1103/PhysRevE.57.7192).
- [19] A. P. Thompson, S. J. Plimpton, W. D. Mattson, General formulation of pressure and stress tensor for arbitrary many-body interaction potentials under periodic boundary conditions., *The Journal of chemical physics* 131 15 (2009) 15410.
- [20] P. L. Barclay, D. Z. Zhang, Periodic boundary conditions for arbitrary deformations in molecular dynamics simulations, *Journal of Computational Physics* 435 (2021) 110238. doi:<https://doi.org/10.1016/j.jcp.2021.110238>.
URL <https://www.sciencedirect.com/science/article/pii/S0021999121001339>
- [21] D. An, S. Y. Cheng, T. Head-Gordon, L. Lin, J. Lu, Convergence of stochastic-extended lagrangian molecular dynamics method for polarizable force field simulation, *Journal of Computational Physics* 438 (2021) 110338. doi:<https://doi.org/10.1016/j.jcp.2021.110338>.
URL <https://www.sciencedirect.com/science/article/pii/S0021999121002333>
- [22] S. Sastry, The relationship between fragility, configurational entropy and the potential energy landscape of glass-forming liquids, *Nature* 409 (2000) 164–167.
URL <https://api.semanticscholar.org/CorpusID:4392200>
- [23] A. Heuer, Exploring the potential energy landscape of glass-forming systems: from inherent structures via metabasins to

- macroscopic transport, *Journal of Physics: Condensed Matter* 20 (2008) 373101.
URL <https://api.semanticscholar.org/CorpusID:39081030>
- [24] M. C. Payne, M. P. Teter, D. C. Allan, T. A. Arias, J. D. Joannopoulos, Iterative minimization techniques for ab initio total-energy calculations: molecular dynamics and conjugate gradients, *Rev. Mod. Phys.* 64 (1992) 1045–1097. doi:10.1103/RevModPhys.64.1045.
URL <https://link.aps.org/doi/10.1103/RevModPhys.64.1045>
- [25] C. E. Maloney, A. Lemaitre, Amorphous systems in athermal, quasistatic shear., *Physical review. E, Statistical, nonlinear, and soft matter physics* 74 1 Pt 2 (2005) 016118.
- [26] A. Zaccone, Elastic deformations in covalent amorphous solids, *Modern Physics Letters B* 27 (2013) 1330002.
URL <https://api.semanticscholar.org/CorpusID:123426572>
- [27] A. Zaccone, E. M. Terentjev, Disorder-assisted melting and the glass transition in amorphous solids., *Physical review letters* 110 17 (2012) 178002.
URL <https://api.semanticscholar.org/CorpusID:15600577>
- [28] L. Verlet, Computer "experiments" on classical fluids. i. thermodynamical properties of lennard-jones molecules, *Phys. Rev.* 159 (1967) 98–103. doi:10.1103/PhysRev.159.98.
- [29] M. Tsamados, A. Tanguy, C. Goldenberg, J.-L. Barrat, Local elasticity map and plasticity in a model lennard-jones glass., *Physical review. E, Statistical, nonlinear, and soft matter physics* 80 2 Pt 2 (2009) 026112.
URL <https://api.semanticscholar.org/CorpusID:31707575>
- [30] J. E. Jones, S. Chapman, On the determination of molecular fields.—i. from the variation of the viscosity of a gas with temperature, *Proceedings of the Royal Society of London. Series A, Containing Papers of a Mathematical and Physical Character* 106 (738) (1924) 441–462. doi:10.1098/rspa.1924.0081.
- [31] D. Frenkel, B. Smit, *Understanding molecular simulation: From algorithms to application.*, Academic Press, San Diego, 2001.
- [32] S. Nosé, F. Yonezawa, Isothermal–isobaric computer simulations of melting and crystallization of a lennard-jones system, *Journal of Chemical Physics* 84 (1986) 1803–1814.
URL <https://api.semanticscholar.org/CorpusID:95892095>
- [33] Y.-Q. Jiang, P. Peng, Nearly golden-ratio order in ta metallic glass*, *Chinese Physics B* 29 (4) (2020) 046105. doi:10.1088/1674-1056/ab773f.
URL <https://dx.doi.org/10.1088/1674-1056/ab773f>
- [34] W. G. Hoover, Canonical dynamics: Equilibrium phase-space distributions, *Phys. Rev. A* 31 (1985) 1695–1697. doi:10.1103/PhysRevA.31.1695.
URL <https://link.aps.org/doi/10.1103/PhysRevA.31.1695>
- [35] S. Melchionna, G. Ciccotti, B. L. H. and, Hoover npt dynamics for systems varying in shape and size, *Molecular Physics* 78 (3) (1993) 533–544. doi:10.1080/00268979300100371.
- [36] M. P. Allen, D. J. Tildesley, *Computer Simulation of Liquids*, Oxford University Press, 2017. doi:10.1093/oso/9780198803195.001.0001.
- [37] F. D. Di Tolla, M. Ronchetti, Applicability of nosé isothermal reversible dynamics, *Phys. Rev. E* 48 (1993) 1726–1737. doi:10.1103/PhysRevE.48.1726.
URL <https://link.aps.org/doi/10.1103/PhysRevE.48.1726>
- [38] Hünenberger, P. H., *Thermostat Algorithms for Molecular Dynamics Simulations*, Springer Berlin Heidelberg, Berlin, Heidelberg, 2005, Ch. 2, pp. 105–149. doi:10.1007/b99427.
- [39] J.-L. Lions, Y. Maday, G. Turinici, Résolution d'edp par un schéma en temps "pararéel", *Comptes Rendus de l'Académie des Sciences - Series I - Mathematics* 332 (7) (2001) 661–668. doi:[https://doi.org/10.1016/S0764-4442\(00\)01793-6](https://doi.org/10.1016/S0764-4442(00)01793-6).
- [40] F. Bamer, F. Ebrahim, B. Markert, B. Stamm, Molecular mechanics of disordered solids, *Archives of Computational Methods in Engineering* 30 (3) (2023) 2105–2180. doi:10.1007/s11831-022-09861-1.
- [41] J. Bezanson, A. Edelman, S. Karpinski, V. B. Shah, Julia: A fresh approach to numerical computing, *SIAM review* 59 (1) (2017) 65–98.
URL <https://doi.org/10.1137/141000671>
- [42] M. Reihn, F. Bamer, S. S. Alshabab, Z. Wu, *Jumol*, GitHub (2023).
URL <https://github.com/maximilianreihn/Jumol>